Analytical expressions for the luminescence of dilute quaternary InAs(N,Sb) semiconductors

ORIAKU, Chijioke I., SPENCER, Timothy <http://orcid.org/0000-0003-1135-4042>, YANG, X., ZUBELLI, J.P. and PEREIRA, Mauro <http://orcid.org/0000-0002-2276-2095>

Journal of Nanophotonics

Nanophotonics.SPIEDigitalLibrary.org

Analytical expressions for the luminescence of dilute quaternary InAs(N,Sb) semiconductors

Chijioke I. Oriaku
Timothy J. Spencer
Xu Yang
Jorge P. Zubelli
Mauro F. Pereira

SPIE.

Chijioke I. Oriaku, Timothy J. Spencer, Xu Yang, Jorge P. Zubelli, Mauro F. Pereira, "Analytical expressions for the luminescence of dilute quaternary InAs(N,Sb) semiconductors," *J. Nanophoton.* **11**(2), 026005 (2017), doi: 10.1117/1.JNP.11.026005.

Analytical expressions for the luminescence of dilute quaternary InAs(N,Sb) semiconductors

Chijioke I. Oriaku,[a,b] Timothy J. Spencer,[a] Xu Yang,[c] Jorge P. Zubelli,[c] and Mauro F. Pereira[a,*]

[a]Sheffield Hallam University, Materials and Engineering Research Institute, Sheffield, United Kingdom

[b]Michael Okpara University of Agriculture, Department of Physics, Umudike, Nigeria

[c]Instituto de Matemática Pura e Aplicada, Rio de Janeiro, Brazil

Abstract. We calculate the luminescence of the dilute quaternary InAs(N,Sb). The incorporation of N leads to a reduction of the energy gap of the host InAs and Sb acts as a surfactant, improves the N incorporation, and further reduces the bandgap. This is thus extremely relevant for devices operating in the mid-infrared (MIR) spectral range from 3 to 5 μm. In order to describe this system, the theory starts with the band anticrossing model applied to both conduction and the valence band to generate inputs for analytical approximations that lead to luminescence spectra, including plasma screening, bandgap renormalization, and excitonic enhancements. Direct application of the equations leads to good agreement with some recent experimental data. © *2017 Society of Photo-Optical Instrumentation Engineers (SPIE)* [DOI: 10.1117/1.JNP.11.026005]

Keywords: photoluminescence; dilute semiconductors; many body effects.

Paper 17008 received Feb. 5, 2017; accepted for publication Mar. 29, 2017; published online May 3, 2017.

1 Introduction

Photoluminescence, or more generally, photon emission due to different excitation processes[1,2] is a very powerful tool to characterize semiconductor materials and map specific characteristics of new devices,[3,4] notably dilute semiconductor materials, which have strong potential for light-harvesting devices and one of the most widely studied dilute semiconductors is InAsN.[5–8] Similar to other III–V dilute semiconductors, InAsN exhibits a very large energy bandgap bowing, which is due to the remarkable variations in the atomic sizes and electronegativity[9] between the nitrogen and InAs. This results in the substitution of a small fraction of the N atoms for InAs and hence the conduction band (CB) is perturbed by the N-impurity localized state, which is usually below the CB edge of InAs. The mechanism of the resulting CB edge reduction has been explained by the so-called CB anticrossing model.[10,11] A further improvement has been reported[6,7] on the spectral qualities of InAsN by the introduction of Sb ions. This yields a narrower bandgap InNAsSb alloy semiconductor and has been successfully done using Sb flux in molecular beam epitaxy and a redshift in bandgap on the incorporation of Sb has been reported.[9] Furthermore, bandgap engineering by incorporating Sb ions is known to deliver emission at the spectral range between 3 and 5 μm. Thus, devices based on these alloys are potential candidates in medical diagnostics, free-space communication, and atmospheric pollution sensors.[12,13] Also, strained InAsNSb epilayers on InAs substrate for LED applications have been reported.[6] Just as the presence of the N impurity reduces the CB edge, the incorporation of Sb increases the valence band (VB) edge thereby causing a further reduction in the bandgap.[12] In fact, it has been noted that the roles of Sb in InAsN are to serve as a surfactant[6,9] and also that when a little amount is incorporated into the lattice it can be used to tune the bandgap of InAs(N,Sb).[6] Hence InNAsSb alloys have huge potential for the development of optoelectronic devices operating in mid-infrared (MIR) spectral range from 3 to 5 μm, to be used in a large number of applications including

*Address all correspondence to: Mauro F. Pereira, E-mail: m.pereira@shu.ac.uk

1934-2608/2017/$25.00 © 2017 SPIE

medical diagnostics, atmospheric pollution monitoring, and free-space communication. The more complex band anticrossing model required to describe the band structure of InAs(N, Sb), where both conduction and valence can be engineered and tailored to specific applications, must then be included in an approach such as that found in simpler systems, such as in Ref. 14. This is achieved in this paper, which is organized as follows: we start with a description of the band structure solution and show how it is included in the luminescence solver. Next, direct comparisons with experiments in the literature are used to validate the model for different quaternary concentrations. The combined role of plasma screening, bandgap renormalization, and excitonic enhancement are put in evidence by comparing and contrasting calculations including these many body effects and the experiments against the free carrier case. These effects have been included, because they are sufficient to explain the experimental data, without introducing extra momentum dependence that would prevent the development of simple analytical solutions, which are a target for an approach that can be easily used by a large number of colleagues. A brief summary follows.

2 Outline of the Mathematical Model and Material Properties

2.1 *Band Structure*

The incorporation of Sb in an InAsN semiconductor yields an alloy of the form $InAs_{1-x-y}N_xSb_y$. Here, x and y are N and Sb mole fractions, respectively. In the treatment of the bandgap energy of $InAs_{1-x-y}N_xSb_y$ alloy, the band anticrossing model is applied on the CB and the VB since the reduction of the bandgap energy is due to the presence of both N and Sb impurities. At the CB, N is substituted in small amount for the As^- atom in the binary InAs introducing an N^- isoelectronic level. A similar approach has been applied in the study of GaAsNSb.[9] The solutions of the resulting dispersive eigenstates give doubly degenerate subbands described by the CB anticrossing model (BAC)

$$E_{\pm}^{C}(k)=\frac{1}{2}\left\{E^{N}+E_{C,\mathrm{InAs}}(k)\pm\sqrt{[E^{N}-E_{C,\mathrm{InAs}}(k)]^{2}+4V_{N}^{2}x}\right\}, \tag{1}$$

where E^{N}, $E_{C,\mathrm{InAs}}$, and V_{N} are the N^- isoelectric level, CB edge energy, and the matrix element describing the coupling constant between the N^- impurity level and the extended CB state. Similarly, in the VB, the presence of the Sb atom introduces an impurity state below the VB maximum of InAs. This supports the application of the result of a 12×12 band $k\cdot p$ method[15] for VB anticrossing model with the subband energy eigenvalues

$$E_{\pm}^{\mathrm{hh}}(k)=\frac{1}{2}[E^{\mathrm{Sb}}+H\pm\sqrt{(E^{\mathrm{Sb}}-H)^{2}+4V_{\mathrm{Sb}}^{2}y}], \tag{2}$$

$$E_{\pm}^{\mathrm{lh}}(k)=\frac{1}{2}[E^{\mathrm{Sb}}+L\pm\sqrt{(E^{\mathrm{Sb}}-L)^{2}+4V_{\mathrm{Sb}}^{2}y}], \tag{3}$$

$$E_{\pm}^{\mathrm{SO}}(k)=\frac{1}{2}[E^{\mathrm{Sb-SO}}+S\pm\sqrt{(E^{\mathrm{Sb-SO}}-S)^{2}+4V_{\mathrm{Sb}}^{2}y}], \tag{4}$$

where H and L denote the VB energies for the heavy-holes (hh) and light hole (lh) band, respectively, band of the binary InAs semiconductor. The spin orbit split-off energy (SO) is denoted by S. Within the 12×12 $k\cdot p$ band, the energies are given as, $H=-\hbar^2k^2/2m_{\mathrm{hh}}+\Delta E_{\mathrm{VBM}}y$, $L=-\hbar^2k^2/2m_{\mathrm{lh}}+\Delta E_{\mathrm{VBM}}y$, and $S=(H+L)-\Delta_0-\Delta E_{\mathrm{SO}}y$, respectively, where Δ_0, m_{lh}, and m_{hh} are the spin orbit, light-hole, and heavy-hole effective masses of InAS semiconductor. The impurity levels of the heavy holes and the spin orbit split-off bands are denoted by E^{Sb} and $E^{\mathrm{Sb-SO}}$, respectively. The matrix element for the coupling constant that describes the interaction between Sb and the VB states is denoted by V_{Sb}. The theoretical value of the bandgap of the quaternary $InAs_{1-x-y}N_xSb_y$ alloy can thus be obtained taking into account the virtual crystal approximation (VCA), as the difference between the band extrema E^c and E^v. In this case,

the band extrema are given as $E^c = E^c_- - \Delta E_C$ and $E^v = E^{\mathrm{hh}}_+ - \Delta E_V$, where ΔE_C and ΔE_V are the conduction and VB discontinuities between the end point binaries, i.e., InAs and InSb. The VB positions $E_{v,\mathrm{InAs}}$ and $E_{v,\mathrm{InSb}}$ of the binaries InAs and InSb can be calculated[16] by using $E_{v,\mathrm{InAs}} = E_{vav,\mathrm{InAs}} + \Delta_{0,\mathrm{InAs}}/3$ and $E_{v,\mathrm{InSb}} = E_{vav,\mathrm{InSb}} + \Delta_{0,\mathrm{InSb}}/3$. Their corresponding CB positions are $E_{c,\mathrm{InAs}} = E_{v,\mathrm{InAs}} + E_{g,\mathrm{InAs}}$ and $E_{c,\mathrm{InSb}} = E_{v,\mathrm{InSb}} + E_{g,\mathrm{InSb}}$, respectively. The spin orbit split-off energy position is calculated $E_{\mathrm{SO,InAs}} = E_{vav,\mathrm{InAs}} - 2\Delta_{0,\mathrm{InAs}}/3$ and $E_{\mathrm{SO,InSb}} = E_{vav,\mathrm{InSb}} - 2\Delta_{0,\mathrm{InSb}}/3$. Here, E_{vav} and Δ_0 represent the average valence subband and spin orbit energy of InAs or InSb semiconductor, respectively. The conduction, valence, and spin orbit split-off band discontinuities between the binaries InAs and InSb are then, respectively, evaluated as $\Delta E_C = E_{c,\mathrm{InAs}} - E_{c,\mathrm{InSb}}$, $\Delta E_v = E_{v,\mathrm{InSb}} - E_{v,\mathrm{InAs}}$, and $\Delta E_{\mathrm{SO}} = E_{\mathrm{SO,InSb}} - E_{\mathrm{SO,InAs}}$.

2.2 *Luminescence*

The optical response of semiconductor materials can be obtained by self-consistent evaluation of many body nonequilibrium Green's functions (NEGF), which have been successfully applied to intersubband[11,17,18] and interband transitions[19,20] in quantum wells and superlattices. This paper starts from an approach that can also describe superlattices as effective 3-D anisotropic media[21] and leads to very accurate approximations. Here, the band structure relations described in Sec. 2.1 are inserted in the analytical solution for semiconductor luminescence, which has been derived in Ref. 14 by means of a step by step set of approximations applied to the equation for the interband polarization, within the context of a microscopic NEGF formalism

$$I(\omega) = I_0 \left[\frac{\hbar\omega}{E_0}\right]^3 \frac{1}{e^{\beta(\hbar\omega-\mu)}+1} \left\{ \sum_{l=1}^{g^{1/2}} \frac{4\pi}{l} \left[\frac{1}{l^2} - \frac{l^2}{g^2}\right] \delta_\Gamma\left(\Delta - \frac{E_l}{E_0}\right) + 2\pi \int_0^\infty \mathrm{d}\varphi \frac{\sinh \pi g\sqrt{\varphi}}{\cosh \pi g\sqrt{\varphi} - \cosh \pi\sqrt{\varphi g^2 - 4}\, g} \delta_\Gamma(\Delta - \varphi) \right\}, \tag{5}$$

where $I_0 = |\wp|^2 E_0^2 n_b/\pi^2\hbar^3 c^3 a_0^3$, $\wp$, n_b, c, E_0, and a_0 are the dipole matrix element, background refractive index, speed of light in vacuum, exciton binding energy, and Bohr radius, respectively. ϕ, β, and μ are the integration variable, inverse thermal energy, and quasiparticle chemical potential with respect to the bandgap energy of the dilute nitride material E_g. The probe photon energy $\hbar\omega$ is detuned by $\Delta = \hbar\omega - E_g/E_0$, where E_g is renormalized, following the standard Mott criterion as reported in Ref. 21. The bound state energies are given as $E_l = -E_0(l^{-1} - g^{-1}l)^2$. The integral runs from $l = 1$ through the square root of the band state factor g. The optical properties depend largely on the bandgap of the quaternary alloy, which is influenced by Sb and N mole fractions. In fact, one would expect a much stronger dependence on N mole ratio than Sb mole since it is only a small part of the latter that enters the lattice of the quaternary alloy.[8] The distribution of the N mole fraction x is expected to cause an inhomogeneous broadening of the photoluminescence spectra of $\mathrm{InAs}_{1-x-y}\mathrm{N}_x\mathrm{Sb}_y$ alloy. Here, the inhomogeneously broadened luminescence is approximated as a statistical average of the homogeneously broadened luminescence spectra

$$I_{\mathrm{inh}}(\omega) = \int_{-\infty}^{\infty} I(\omega, x) G(x) \mathrm{d}x, \tag{6}$$

where $G(x)$ is the Gaussian linewidth having a nominal N^- mole fraction x_0 and standard deviation σ_x given by $G(x) = 1/\sqrt{2\pi}\sigma_x e^{-[(x-x_0)/2\sigma_x^2]}$. Details of all expressions above are given in Ref. 14. The goal of this paper is to extend the approach to quaternary materials and describe corresponding experimental results. In the simulations presented next, we just considered a distribution $G(x)$ (nitrogen related) and let y (Sb) be a fixed parameter.

3 Numerical Results and Discussions

In our calculations, the N impurity level is taken with the form $E^{\mathrm{N}} = E^{\mathrm{N0}} - \alpha x$, where the value $E^{\mathrm{N0}} = 1.48$ eV,[9] instead of the tight binding approximation values of $E^{\mathrm{N0}} = 1.36$ eV in Ref. 5,

using $\alpha = 2$ from Refs. 5 and 9. The free fitting parameter V_N is taken as $V_N = 2$ eV, following Ref. 22. The position of the Sb level $E^{Sb} = 1.0$ eV (Ref. 10) the corresponding spin orbit splitting energy impurity level, $E^{Sb-S0} = 1.6$ eV, and the free parameter for the VB $V_{Sb} = 1.05$ eV were used in the calculations.[10,23] Figure 1 shows the schematic diagram of the band lineup of $InAs_{1-x-y}N_xSb_y$ using the BAC model.

The CB minimum is controlled by the N^- mole fractions and the VB maximum is controlled by the Sb^- mole fraction. The VCA is used to introduce the small band offsets ΔE_C and ΔE_V between the constituent InAs and InSb. At zero doping level, i.e., $y = 0$ and $x = 0$, the bandgap of the semiconductor is simply $E_{g,InAs}$ as depicted in the diagram above. The material is completely InAsN when the Sb mole fraction is $y = 0$ and the N^- mole fraction is increased to a small amount x. In this case, the band offsets are zero and the VB maximum will be that of InAs, instead of InAsSb as can be seen in the diagram. A narrower bandgap $InAs_{1-x-y}N_xSb_y$ is obtained when both Sb and N^- impurities are present. Figures 2(a) and 2(b) below depict the band structure of $InAs_{1-x-y}N_xSb_y$ with a lattice temperature of 295 K, calculated for the mole fraction combinations (a) 1.4% N, 4.1% Sb and 1.8% N, and 7.3% Sb. The plots show the dispersions as depicted in Eqs. (1) to (3) above. The dotted lines show the dispersions of the host binary semiconductor, whereas the solid lines show the corresponding dispersions of dilute quaternary semiconductor. The relevance of our approach compared to Bose–Einstein

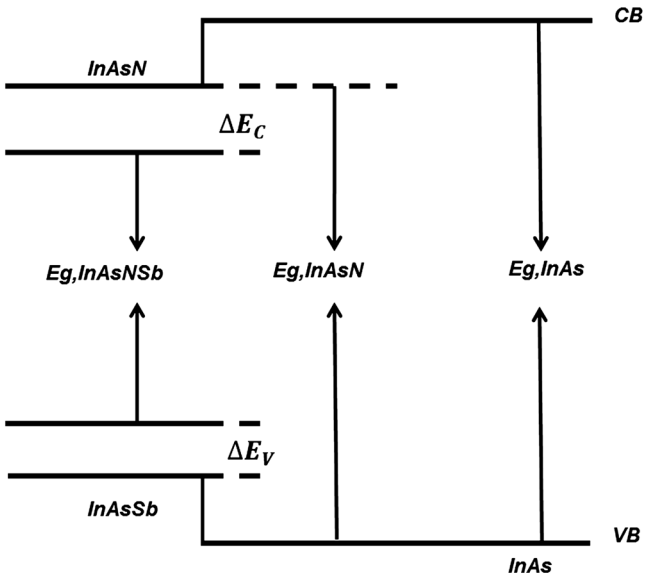

Fig. 1 Band schematics of $InAs_{1-x-y}N_xSb_y$ dilute semiconductors.

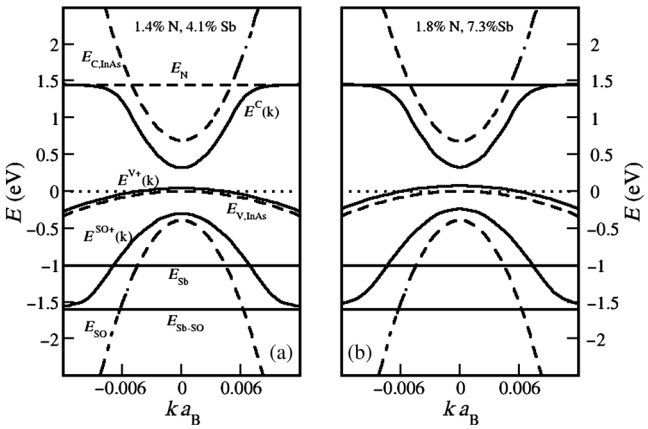

Fig. 2 Band structure of (a) 1.4%, 4.1% and (b) 1.8%, 7.3%. The incorporation of Sb promotes a further reduction in bandgap, although the prominent shrinkage is due to N.

($E_{g,\mathrm{BE}}$) and Varshini ($E_{g,\mathrm{Var}}$) fits to the bandgap are made clear later in the text when we directly compare free carrier approximations, many body corrections, and the fits themselves. These fits are characterized by the following parameters and expressions

$$E_{g\,\mathrm{Var}} = E_{g0} - \frac{\alpha T^2}{T+\beta}, E_{g\,\mathrm{BE}} = E_{g0\,\mathrm{BE}} - \frac{2a_B}{\exp\left(\frac{\theta_B}{T}\right) - 1}. \tag{7}$$

Figure 3 compares the computed and experimentally measured luminescence for the different mole fractions.

Using the inhomogeneously broadened luminescence given in Eq. (6) above, a simple Gaussian distribution with standard deviation $\sigma_x = 0.0025$ was sufficient to obtain a spectrum with a reasonable linewidth. All through the calculations, the density used was $n = 10^{14}$ carriers/cm^3. The calculated luminescence spectra are in good agreement with the reported experimental results in Ref. 5. Figure 4 shows the luminescence spectra at different carrier temperatures for two different sample compositions.

The required dependence of the free carrier energy bandgaps with temperature are given by the Varshni relation for the host binary material InAs given in Ref. 24, where E_{g0} is the low-temperature bandgap of binary InAs $E_{g0} = 417$ meV, α and β are the Varshni parameters given by $\alpha = 0.276$ meV/K^2, $\beta = 93$ K [see Eq. (7)]. In order to highlight the relevance of our approach, Fig. 5 depicts the luminescence energy peaks with respect to temperature for the sample with 1.4% N and 4.1% Sb.

The calculated emission peaks (black circles) with our approach containing many body effect are in good agreement with the experimentally measured luminescence energy emission peaks (red triangles).[5] The blue circles in Fig. 5 depict the free carrier luminescence at different temperatures that dominate the entire spectrum when the bound state factor $g \to 0$. For both the calculated and experimentally observed luminescence, a blue shift is initially observed at low temperatures ~10 to 80 K before a gradual redshift at higher temperatures. The low-temperature blue shift is due to exciton ionization, showing clearly the importance of our approach. The solid (red) and dashed (green) curves were calculated, respectively, with Bose–Einstein and Varshini fits to the bandgap for a comparison. The strong deviations at a higher temperature further highlight the relevance of our approach and our choice of bandgap calculation, which reflects directly on the free carrier curve and the further improvement in agreement with experiments due to the combined effect of plasma screening, bandgap renormalization, and excitonic enhancement in our many body calculations. The combination of the method presented here with other more

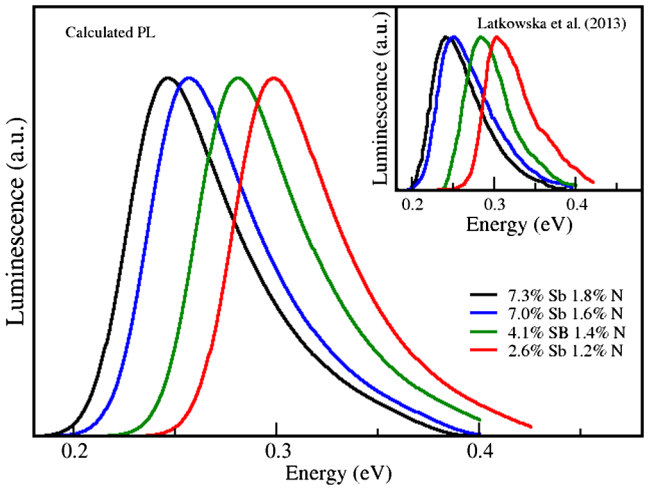

Fig. 3 Room temperature luminescence of dilute semiconductor. The plots are the calculated luminescence spectra and the inset plots are the measured luminescence extracted from Ref. 5. The lines are (from left to right): 1.8%, 7.3% (blue); 1.6%, 7.0% (green); 1.4%, 41% (red); and 1.2%, 2.6% (cyan). The theory predicts the general feature of a strongly asymmetric spectral shape at room temperature in good agreement with experiments.

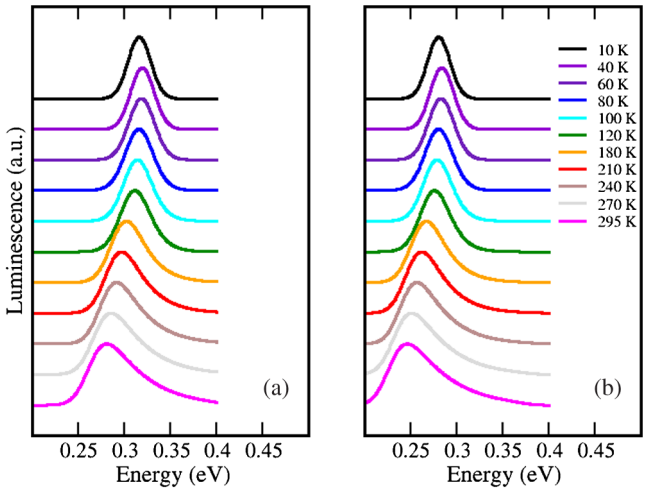

Fig. 4 Calculated luminescence of. (a) 1.4%, 4.1% and (b) 1.8%, 7.3% for different temperatures increasing from 10 to 295 K. The evolution from a Gaussian-like shape at low temperature to an asymmetric shape at high temperature is a general feature in excellent agreement with the experimental spectra reported in Fig. 2 of Ref. 5.

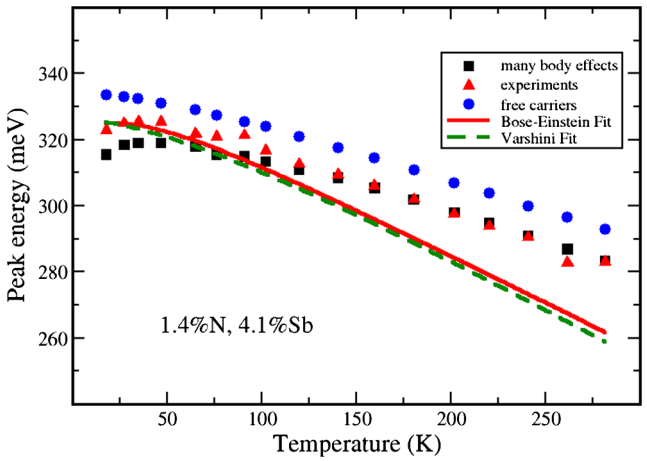

Fig. 5 Temperature dependence of the peak luminescence of for the mole fractions 1.4%, 4.1%. The black squares are calculated with our many body approach, blue circles are for free carriers, and the red triangles are experimental data extracted from Ref. 5 for comparison. The red solid and green dashed curves are the Bose–Einstein and Varshini fits for the bandgaps with parameters given in Ref. 5. The Varshini and Bose–Einstein parameters of the fit Eq. (7) for the quaternary are also given in Ref. 5: $E_{g0} = 326$ meV, $\alpha = 0.328$ meV/K^2, $\beta = 106$ K, $E_{g0\mathrm{BE}} = 325$ meV, $a_\mathrm{B} = 20$ meV, and $\theta_\mathrm{B} = 138$ K.

fundamental band structure calculations beyond $k \cdot p$ (Ref. 25) can lead to a very powerful predictive numerical tool to be used in the development of new materials and devices, notably dilute semiconductor lasers.[26]

4 Conclusion

We have presented in this paper theoretical calculations of luminescence emission in dilute quaternary semiconductors of type $InAs_{1-x-y}N_xSb_y$. The band structure was obtained by applying the conduction and VB anticrossing model on the nitrogen modified CB and the Sb modified VB. Good agreement is obtained by comparing simulations and experimental findings of the evolution of spectra with different alloy compositions. The role of the combined effect of plasma screening, bandgap renormalization, and excitonic enhancement was demonstrated by

comparing and contrasting calculations including these many body effects and the experiments against the free carrier case. The reason for including only these effects among further possibilities of other many body corrections is that they are sufficient to explain the experimental data, without introducing extra momentum dependence that would prevent the development of simple analytical solutions, which are a target for an approach that can be easily used by a large number of colleagues and are relatively easily programmed. Thus, this work has potential to support the numerical characterization of new semiconductor layers developed for devices targeting the midinfrared range.

Acknowledgments

The authors acknowledge the support from MPNS COST ACTION MP1204—TERA-MIR Radiation: Materials, Generation, Detection, and Applications and COST ACTION BM1205 European Network for Skin Cancer Detection using Laser Imaging. C. I. Oriaku's research was supported by TETFUND, Nigeria. T. J. Spencer's research was supported by the Grant No. EP/M006948/1 from the EPSRC.

References

1. H. Ouerdane et al., "Photon emission induced by elastic exciton-carrier scattering in semiconductor quantum wells," *Eur. Phys. J. B* **65**(2), 195–206 (2008).
2. M. E. Portnoi and I. Galbraith, "Ionization degree of the electron-hole plasma in semiconductor quantum wells," *Phys. Rev. B* **60**(8), 5570–5581 (1999).
3. A. Wójcik et al., "Photoluminescence mapping and angle-resolved photoluminescence of MBE-grown InGaAs/GaAs RC LED and VCSEL structures," *Thin Solid Films* **412** (1–2), 114–121 (2002).
4. A. Wojcik-Jedlinska et al., "Optical characterisation of vertical-external-cavity surface-emitting lasers (VECSELs)," *Opt. Appl.* **37**(4), 449–457 (2007).
5. M. Latkowska et al., "Temperature dependence of photoluminescence from InNAsSb layers: The role of localized and free carrier emission in determination of temperature dependence of energy gap," *Appl. Phys. Lett.* **102**(12), 122109 (2013).
6. Q. Zhuang et al., "Molecular beam epitaxial growth of InAsN: Sb for midinfrared Optoelectronics," *Appl. Phy. Let.* **93**(12), 121903 (2008).
7. R. Kudrawiec et al., "Photoreflectance study of N- and Sb-related modifications of the energy gap and spin-orbit splitting in InNAsSb alloys," *Appl. Phys. Lett.* **99**(1), 011904 (2011).
8. R. Chen et al., "Photoluminescence properties of midinfrared dilute nitride InAsN epilayers with/without Sb flux during molecular beam epitaxial growth," *Appl. Phys. Lett.* **95**(26), 261905 (2009).
9. T. D. Veal et al., "Photoluminescence spectroscopy of bandgap reduction in dilute InNAs alloys," *Appl. Phys. Lett.* **87**(18), 182114 (2005).
10. Y. T. Lin et al., "Energy gap reduction in dilute nitride GaAsSbN," *Appl. Phys. Lett.* **93**(17), 171914 (2008).
11. M. F. Pereira, "The linewidth enhancement factor of intersubband lasers: From a two-level limit to gain without inversion conditions," *Appl. Phys. Lett.* **109**(22), 222102 (2016).
12. M. F. Pereira, "TERA-MIR radiation: materials, generation, detection and applications," *Opt. Quantum Electron.* **46**(4), 491–493 (2014).
13. M. F. Pereira, "TERA-MIR radiation: materials, generation, detection and applications II," *Opt. Quantum Electron.* **47**(4), 815–820 (2015).
14. A. I. Oriaku and M. F. Pereira, "Analytical solutions for semiconductor luminescence including Coulomb correlations with applications to dilute bismides," *J. Opt. Soc. Am. B* **34**(2), 321–328 (2017).
15. K. Alberi et al., "Valence-band anticrossing in mismatched III-V semiconductor alloys," *Phys. Rev. B* **75**(4), 045203 (2007).
16. S L Chuang, *Physics of Photonic Devices*, 2nd ed., John Wiley & Sons, New York (2009).

17. M. F. Pereira, "Microscopic approach for intersubband-based thermophotovoltaic structures in the terahertz and mid-infrared," *J. Opt. Soc. Am. B* **28**(8), 2014–2017 (2011).
18. M. F. Pereira and I. A. Faragai, "Coupling of THz radiation with intervalence band transitions in microcavities," *Opt. Express* **22**(3), 3439–3446 (2014).
19. M. F. Pereira, R. Binder, and S. W. Koch, "Theory of nonlinear optical absorption in coupled-band quantum wells with many-body effects," *Appl. Phys. Lett.* **64**(3), 279–281 (1994).
20. H. Grempel et al., "High-density effects, stimulated emission, and electrooptical properties of ZnCdSe/ZnSe single quantum wells and laser diodes," *Phys. Status Solidi B* **194**(1), 199–217 (1996).
21. M. F. Pereira, "Analytical solutions for the optical absorption of semiconductor superlattices," *Phys. Rev. B* **52**(3), 1978–1983 (1995).
22. I. Vurgaftman and J. R. Meyer, "Band parameters for nitrogen-containing semiconductors," *J. Appl. Phys.* **94**(6), 3675–3696 (2003).
23. A. Aissat et al., "Effect of on band alignment of compressively strained $Ga_{1-x}In_xN_y$ $As_{1-y-z}Sb_z$/GaAs quantum well structures," *Phys. E* **43**(1), 40–44 (2010).
24. I. Vurgaftman, J. R. Meyer, and L. R. Ram-Mohan, "Band parameters for III-V compound semiconductors and their alloys," *J. Appl. Phys.* **89**(11), 5815–5875 (2001).
25. M. Seifikar, E. P. O'Reilly, and S. Fahy, "Self-consistent Green's function method for dilute nitride conduction band structure," *J. Phys.* **26**(36), 365502 (2014).
26. M. F. Pereira, "The linewidth enhancement factor of intersubband lasers: from a two-level limit to gain without inversion conditions," *Appl. Phys. Lett.* **109**(22), 222102 (2016).

Chijioke I. Oriaku received his PhD from Sheffield Hallam University in 2015. He is a lecturer in the Department of Physics, Michael Okpara University of Agriculture, Umudike, Nigeria. He is the author of 23 publications. His current research interests are focused on the theory of semiconductors.

Timothy J. Spencer received his PhD from Sheffield Hallam University in 2005. He is a research fellow/lecturer in the Materials and Engineering Research Institute, Sheffield Hallam University, UK. He has 19 journal publications and 2 book chapters. He conducts research in numerical methods and has a particular interest in complex fluids.

Xu Yang obtained her PhD from Nankai University, China, in 2011. She is a postdoctoral researcher at the Laboratory for Mathematical Modeling and Analysis in the Applied Sciences (LAMCA) at IMPA. She works in the fields of applied mathematics with emphasis on inverse problems and graph theory. She has coauthored 10 research and technical contributions.

Jorge P. Zubelli obtained his PhD from the University of California at Berkeley, California, in 1989. He is a professor of mathematics at the National Institute for Pure and Applied Mathematics (IMPA), Rio de Janeiro, Brazil, and heads the LAMCA at IMPA. He works on mathematical modeling and inverse problems and coauthored over 80 research and technical contributions.

Mauro F. Pereira obtained his PhD at the Optical Sciences Center, University of Arizona in 1992. He has been a professor and chair of theory of semiconductor materials and optics at the Materials and Engineering Research Institute, Sheffield Hallam University, UK, since 2006. He has over 125 journal and proceeding publications and was elected a fellow of SPIE in 2011 for achievements in theory of semiconductor materials and optics.